CRACK PROPAGATION BEHAVIOUR OF A PUDDLE IRON UNDER CONSTANT AND VARIABLE AMPLITUDE LOADING

A.M. P. de Jesus [1], J.M.C. Maeiro [2], A.L.L. da Silva [3], A.S. Ribeiro [4]

[1]UCVE/IDMEC-FEUP & Departamento de Engenharias, Universidade de Trás-os-Montes e Alto Douro
[2]Departamento de Engenharias, Universidade de Trás-os-Montes e Alto Douro
[3]Unidade de Concepção e Validação Experimental, IDMEC-FEUP
[4]UCVE/IDMEC-FEUP & Departamento de Engenharias, Universidade de Trás-os-Montes e Alto Douro




ABSTRACT

Structural integrity assessments of old steel riveted bridges are more and more frequent. Most of these structures were built between the end of the 19th century and beginning of the 20th century. Fatigue is one major concern for these structures since they show a long operational period with increasing traffic intensity. Despite the S-N approach is widely used to assess the fatigue damage for riveted steel structures, fracture mechanics appears as an alternative approach to perform residual lifetime calculations. Therefore, this paper proposes crack propagation data for a sample of original puddle iron removed from the Portuguese Fão bridge. Constant amplitude crack propagation data is evaluated for several stress R-ratios. The Walker's correction is used to describe the stress R-Ratio effects. Furthermore, crack propagation rates are evaluated for overloading tests. A modified version of the crack propagation model proposed by Wheeler is used to correlate the retardation effects after an overload application.

1- INTRODUCTION

The maintenance and safety of existing bridges is a major concern of governmental agencies. In particular, the safety of old riveted highway and railway bridges fabricated and placed into service at the end of the 19th/ beginning of 20th centuries deserves particular attention, since these bridges were designed taking into account traffic conditions, both in terms of vehicle gross weight and frequency, completely different from those currently observed. Also, the current design procedures were not yet fully developed or even did not exist in the 19th century and designer engineers were not aware of some important phenomena such as fatigue. Fatigue was only intensively studied in the 20th century. In order to assure high safety levels in old riveted steel bridges, highway and railway authorities have to invest heavily in their maintenance and retrofitting.

Despite the S-N approach is widely used to assess the fatigue damage for riveted steel constructions (DiBattista et al. 1998; Geissler 2002; Kulak 2000; Kim et al. 2001), Fracture Mechanics (Wang et al. 2006; Paasch and DePiero 1999) appears as

an alternative approach to perform residual life calculations. Usually, Fracture Mechanics is applied using the well known crack propagation power law proposed by Paris (Paris and Erdogan 1963), supported on constant amplitude crack propagation data. However, and despite its simplicity, it is recognized that the Paris's law shows several limitations, namely it does not account for loading sequential effects, which may be significant in loading histories experienced by bridges. In particular, it is recognized that many materials show a retardation crack growth effect after the application of an overload (Wheeler 1972; Yuen and Taheri 2006; Wang et al. 2009).

This paper presents fatigue crack propagation data for a sample of puddle iron extracted from the road riveted Fão bridge. Constant amplitude fatigue crack growth data is presented for several stress R-ratios. This data is correlated using the Paris's model (Paris and Erdogan 1963). Also, the modification to the Paris's law to account for the stress R-ratio effects, as proposed by Walker (1970) is tested. The constant amplitude crack propagation data is compared with data available for other bridge materials. Fatigue crack growth data is also proposed for the material from the Fão bridge under the action of single overloads. This data is correlated using a modified version of the Wheeler model (Wheeler 1972; Yuen and Taheri 2006; Wang et al. 2009).

2- THE FÃO BRIDGE

The Fão bridge is a riveted metallic road bridge that crosses the Cávado river at Esposende in the northwest region of Portugal. This bridge was inaugurated on 7th August 1892. The bridge has a total length of 267 meters, composed of 8 spans of 33.5 meters each, supported on 7 masonry piers. The material used to build the bridge was puddle iron. Fig. 1 gives a global overview of the bridge.

Recently, the bridge was rehabilitated and some original side diagonals from the bridge (see Fig. 2) were replaced. Specimens required for the experimental work proposed in this paper were extracted from the referred diagonals.

Fig. 1 – Global overview of the Fão Bridge.

Fig. 2 – Diagonals removed from the Fão Bridge.

3- FATIGUE CRACK GROWTH UNDER CONSTANT AMPLITUDE LOADING

Fatigue crack growth tests were conducted according to the ASTM 647 standard (ASTM 1999) using the compact tension (CT) geometry. Fig. 3 illustrates the geometry of the CT specimens that were extracted from the diagonals removed from the Fão bridge.

All tests were performed in air, at room temperature, under a sinusoidal waveform at a maximum frequency of 20 Hz. A total of 12 specimens were tested covering 4 distinct stress R-Ratios, namely R=0, R=0.25, R=0.50 and R=0.75. Crack growth rates were measured using direct optical observations, through a travelling microscope

(0.001 mm resolution). Crack growth was measured on both faces of the specimens.

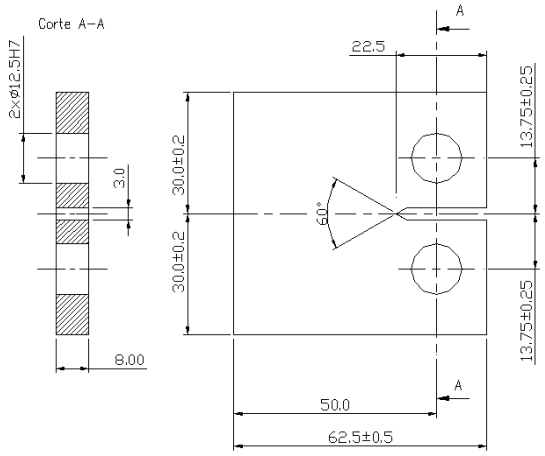

Fig. 3 – Compact tension specimens (dimensions in mm).

Fig. 4 illustrates the crack propagation data for different stress R-ratios. The experimental results were correlated using a power relation between the crack growth rate (*da/dN*) and the stress intensity factor range (ΔK), as proposed by Paris (Paris and Erdogan 1963):

$$\frac{da}{dN} = C\Delta K^{m} \qquad (1)$$

where *da/dN* is the fatigue crack growth rate, ΔK represents the stress intensity factor range and *C* and *m* are material constants. Fig. 4 also includes the Paris's law, resulted from linear regression analysis of log(*da*/*dN*) vs. log(ΔK) data. The respective determination coefficient, R^2, is also shown. The determination coefficient is lower or equal to 0.92, revealing some scatter justified by the heterogeneities typical in the investigated material – a puddle iron. In order to get an idea of the toughness of the material, the maximum stress intensity factor at failure was recorded in each crack propagation test. The average value was 1386 N.mm$^{-1.5}$ with a coefficient of variation of 13.5%. It is interesting to note that the maximum stress intensity factor at failure shows a significant correlation with the stress R-ratio as is illustrated in Fig. 5.

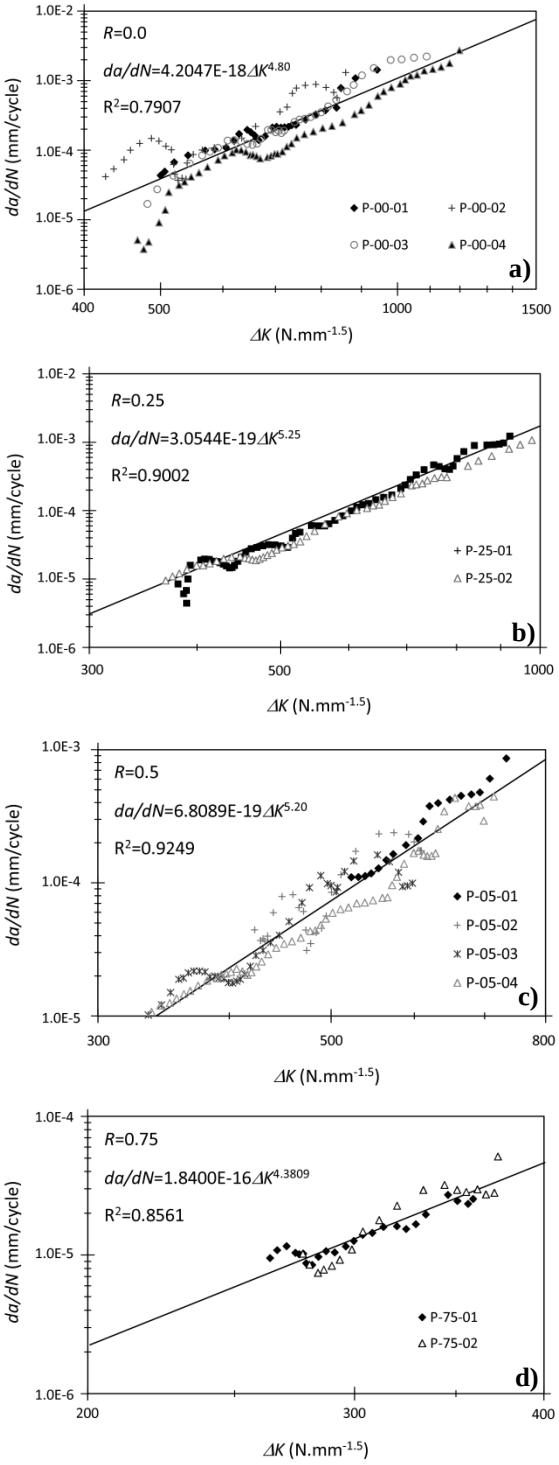

Fig. 4 – Fatigue crack propagation data for several stress R-ratios of the material from the Fão bridge: a) *R*=0.0; b) *R*=0.25; c) *R*=0.5; d) *R*=0.75.

Fig. 6 gathers the crack growth data obtained for the material from the Fão bridge, for all stress ratios. A correlation of all crack growth data is proposed. The resulting scatter is mainly due to the stress R-ratio effect. Fig. 7 compares the regression lines from Fig. 4 and it is clear a stress R-ratio effect on crack

growth. The crack growth rate increases with the stress R-ratio.

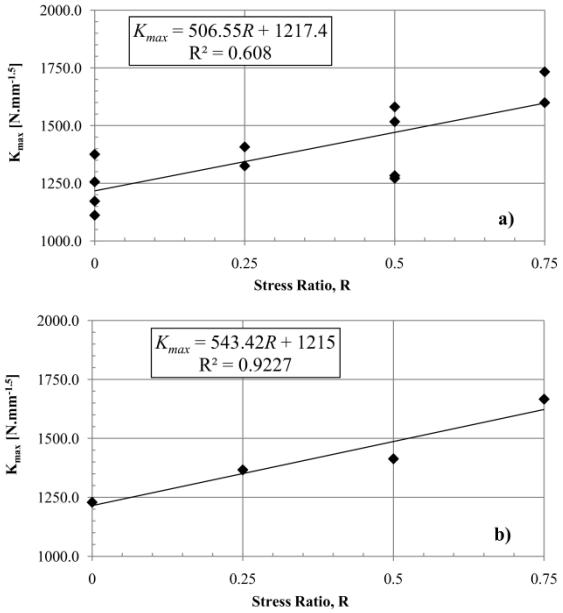

Fig. 5 – Variation of the critical stress intensity factor with the stress R-ratio: a) correlation with all data; b) correlation with average data for each R.

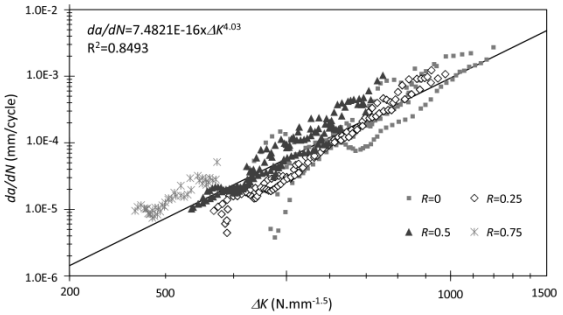

Fig. 6 - Superposition of the crack propagation data from the material of Fão bridge, for distinct stress R-ratios.

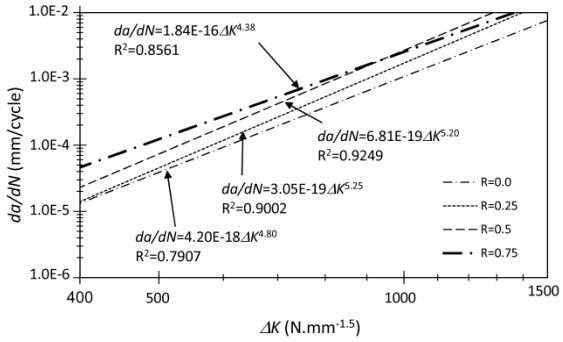

Fig. 7 – Effect of stress R-ratio on crack growth rates (material from Fão bridge).

The Paris's law may be modified to account the stress R-ratio effect. Walker (1970) proposed the following modification in order to take into account the stress R-Ratio effect:

$$\frac{da}{dN} = C\left[\frac{\Delta K}{(1-R)^{1-\gamma}}\right]^m = C\overline{\Delta K}^m \qquad (2)$$

where C, m and γ are empirical parameters to be determined fitting a set of fatigue crack growth data performed at multiple stress R-ratios. Fig. 8 shows the fatigue crack growth data correlated using Eq. (2). The analysis of figure shows a reduction in scatter, since the determination coefficient, R^2, increases from 0.8493 (see Fig. 6) to 0.9126.

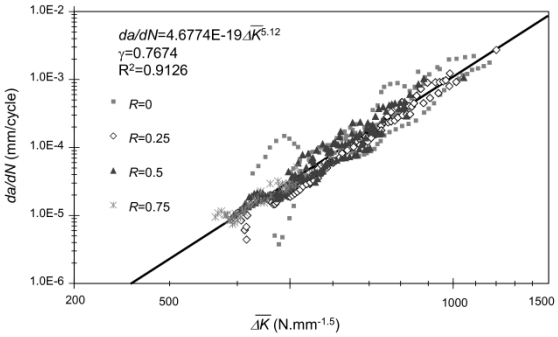

Fig. 8 – Correlation of fatigue crack growth data of the material from Fão bridge, using the Walker model.

Table 1 – Constant amplitude fatigue crack growth constants of the material from the Fão bridge.

Paris's equation			
R-Ratio	C	m	R^2
0.0	4.2047E-18	4.80	0.7907
0.25	3.0544E-19	5.25	0.9002
0.5	6.8089E-19	5.20	0.9249
0.75	1.8400E-16	4.38	0.8561
all	7.4821E-16	4.03	0.8493
Walker's equation			
γ	C	m	R^2
0.7674	4.6774E-19	5.12	0.9126

Note: da/dN in mm/cycle and ΔK in N.mm$^{-1.5}$

In Fig. 9 the constant amplitude fatigue crack growth data obtained for the material from Fão bridge is compared with fatigue crack growth data from materials from

other bridges, such as: Luiz I, Eiffel, Pinhão and Trezói bridges (Correia et al. 2008). It is important to refer that fatigue data from other materials was derived for several stress R-ratios. Fig.9 does not differentiate the several stress R-ratios; only the different materials are discriminated. All data was correlated using the Paris's law resulting a determination coefficient, R^2=0.7417. Two upper bounds of the experimental data were defined which may be useful for design purposes. One curve uses the same slope of the regression line; the other curve uses a slope of 3, the same implicit slope of the S-N curves used in design codes. The material from the Fão bridge shows the higher fatigue crack propagation rates; in the opposite position appears the material from the Eiffel bridge that shows the lower fatigue crack propagation rates. Table 2 summarizes the global average constants of the Paris's relation for the materials from the 5 referred bridges.

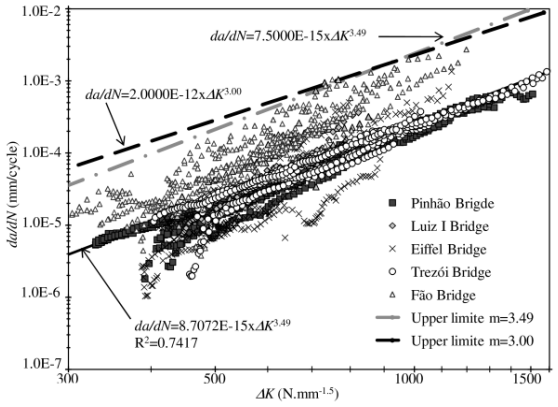

Fig. 9 – Comparison between fatigue crack growth data of several materials from metallic bridges.

Table 2 – Constants of Paris's relation of materials from distinct bridges.

Material/ Bridge	*C*	*m*	R^2
Fão	7.48E-16	4.03	0.8493
Trezói	4.53E-15	3.58	0.9307
Luiz I	2.86E-20	5.50	0.7233
Pinhão	3.20E-15	3.61	0.9618
Eiffel	2.43E-18	4.69	0.7197

Note: *da/dN* in mm/cycle and ΔK in N.mm$^{-1.5}$

4- FATIGUE CRACK GROWTH UNDER VARIABLE AMPLITUDE LOADING

4.1 - Theoretical models

The Paris's law is primarily concerned with fatigue crack propagation under constant amplitude loading. However, loading acting on bridges is essentially of variable amplitude nature (see Fig. 10). The Paris's law is often used to assess variable amplitude loading supported by a damage rule, such as the Miner's linear rule (Miner 1945). This approach may produce satisfactory results for random loading. However, it does not account the fatigue crack growth behaviour for some specific loading conditions, such as overloads as illustrated in Fig. 10a) to Fig. 10c).

Several models have been proposed to consider the overloads effects on crack growth. Wheeler (1972) proposed a model that account for the retardation effects after an overload through the following equation:

$$\frac{da}{dN} = \phi_R . C(\Delta K)^m \qquad (3)$$

where ϕ_R is a retardation parameter. However, more recent studies have proved that crack growth acceleration may occur right after single overload application. Yuen and Taheri (2006) added one more correction to the Wheeler model resulting the following equation:

$$\frac{da}{dN} = \phi_R . \phi_D . C(\Delta K_{acc})^m \qquad (4)$$

where ϕ_R and ϕ_D are two parameters introduced to model the retardation and delayed-retardation growth, respectively; *C* and *m* are identical to those used in the Paris's law (Eq. (1)); ΔK_{acc} is the so-called accelerated stress intensity factor range that will be defined. For stable crack growth, ϕ_R=1, ϕ_D=1, and $\Delta K_{acc} = \Delta K$.

The effect of a single tensile overload is illustrated in Fig. 11. This figure shows the accelerated crack growth that occurs right after a tensile overload, the delay retardation and finally the gradual return to steady state. The three phenomena may be described by Eq. (4).

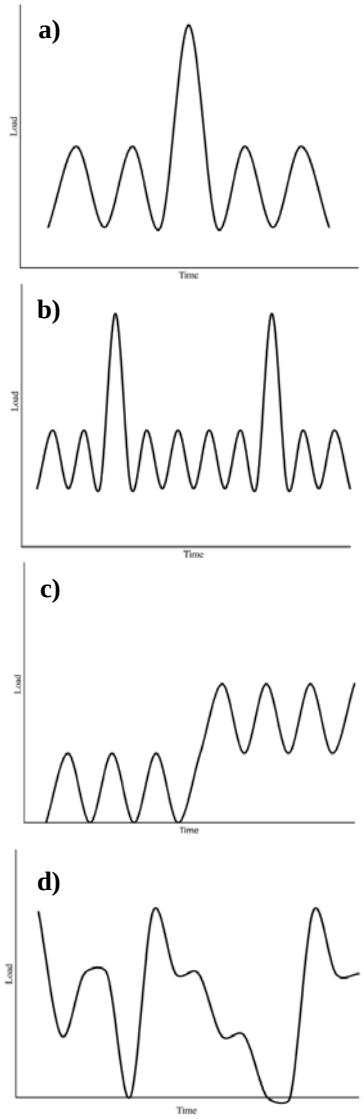

Fig. 10 – Variable amplitude loads: a) single overload; b) periodic overloads; c) loading sequence with increase in stress ratio; d) random loading.

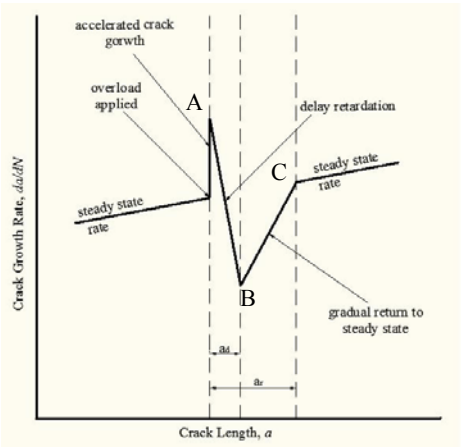

Fig. 11 – Schematic crack growth rate curve showing delayed retardation following a tensile overload (Yuen and Taheri 2006).

The retardation correction factor ϕ_R is defined by:

$$\begin{cases} \phi_R = \left[\dfrac{r_{p,k}}{a_{OL} + r_{p,OL} - a_k} \right]^n \\ if \quad a_k + r_{p,k} < a_{OL} + r_{p,OL} \end{cases} \tag{5.1}$$

or

$$\begin{cases} \phi_R = 1 \\ if \quad a_{OL} + r_{p,OL} \le a_k + r_{p,k} \end{cases} \tag{5.2}$$

where a_k is the current crack length; $r_{p,k}$ is the size of plastic zone created by the post overload constant amplitude loading at a crack length of a_k; n is an adjustable experiment-based shaping exponent; a_{OL} denotes the crack length at which a single tensile overload is applied or a higher loading amplitude is switched to a lower amplitude; $r_{p,OL}$ denotes the size of the plastic zone created by the single tensile overload or the higher loading amplitude in step loading at the crack length of a_{OL} (Wang et al. 2009). The size of the plastic zones may be estimated using the following approach:

$$r_{p,k} = \alpha . \left(\frac{\Delta K_k}{2\sigma_y} \right)^2 \tag{6.1}$$

or

$$r_{p,OL} = \alpha . \left(\frac{K_{OL}}{\sigma_y} \right)^2 \tag{6.2}$$

where σ_y is the yield stress of the material, ΔK_k is the stress intensity factor range at the current crack length a_k and α is the effective plastic zone size constant. If the plane stress condition is postulated, Irwin (1957) states that $\alpha = 1/\pi \cong 0.32$. For plane strain conditions r_p may be 1/3 of the corresponding value for plane stress conditions ($\alpha = 1/3\pi \cong 0.11$). This constant may be experimentally established in order to correlate the total retardation crack length (a_r in Fig. 11), which is the distance over which the retarded crack propagates before the constant amplitude crack growth rate is resumed. The K_{OL} parameter in Eq. (6.2) is defined as follows: for the constant amplitude loading with a single tensile overload, it corresponds to the maximum

value of the overload stress intensity factor, while for the two step high-low loading sequence, K_{OL} is the maximum stress intensity factor of the preceding higher loading step.

The delayed-retardation parameter ϕ_D is defined as:

$$\begin{cases} \phi_D = \left[\dfrac{a_{OL} + r_{D,OL} - a_k}{r_{D,k}} \right]^q \\ if \quad a_k + r_{D,k} < a_{OL} + r_{D,OL} \end{cases} \tag{7.1}$$

or

$$\begin{cases} \phi_D = 1 \\ if \quad a_{OL} + r_{D,OL} \le a_k + r_{D,k} \end{cases} \tag{7.2}$$

where q is an additional shaping parameter; $r_{D,k}$ is the current effective delayed zone size determined by Eq. (6.1), replacing $r_{p,k}$ by $r_{D,k}$; $r_{D,OL}$ denotes the size of the effective delayed zone size, which is related to $r_{p,OL}$ by (Wang et al 2009):

$$r_{D,OL} = \xi \cdot r_{p,OL} \tag{8}$$

where ξ is an experimentally based fitting constant.

The accelerated stress intensity factor range ΔK_{acc} is defined as:

$$\begin{cases} \Delta K_{acc} = \Delta K_k + \\ (\Delta K_{OL} - \Delta K_k).\left(1 - \dfrac{r_{D,k}}{a_{OL} + r_{D,OL} - a_k} \right)^q \\ if \quad a_k + r_{D,k} < a_{OL} + r_{D,OL} \end{cases} \tag{9.1}$$

or

$$\begin{cases} \Delta K_{acc} = \Delta K_k \\ if \quad a_{OL} + r_{D,OL} \le a_k + r_{D,k} \end{cases} \tag{9.2}$$

The stress intensity factor range ΔK_{OL} is set to be $K_{OL}-K_{min}$ for the overloading condition where K_{min} corresponds to the minimum load of the constant amplitude loading (see Fig. 10a)). For a high-low block loading sequence, ΔK_{OL} is set to be the stress intensity factor range ΔK_H of the preceding higher loading step.

Comparing with the Paris's model, the modified Wheeler model defined in Eq. (4) proposes three additional constants, namely n, q and ξ. These constants must be determined from overloading crack growth experiments. The value of n may be estimated by best fitting experimental data in the gradual return to steady state rate behaviour (segment BC in Fig. 11). The value of ξ may be determined by fitting the size of delayed zone AB; q may be estimated by best fitting the crack growth rate in the delayed zone AB. The extension of the segment BC in Fig. 11 is also used to assess the constant α in Eqs. (6). Constants C and m were adjusted considering the steady state fatigue crack propagation for each specimen.

4.2 - Experimental results

In order to identify the constants of the modified Wheeler's model, CT specimens were subjected to simple overloads (see Fig. 10a). A total of three specimens were tested under R=0. The test load was adjusted to result an initial stress intensity factor range, ΔK_i=14 MPa.m$^{0.5}$. The single overload was applied when crack propagates 5 mm from the CT notch root, which means a_{OL}=5+10=15 mm. The ΔK_{OL} was set equal to 1.5ΔK_i. Fig. 12 illustrates the experimental fatigue crack growth data obtained for the three specimens. It is possible to verify some irregularity (instability) in the material response, but the effects of the overload are clearly visible in the graph. The irregularity in the experimental response is due to the heterogeneities in the material, such as slag inclusions. Those heterogeneities may function as a barrier to the crack propagation, producing instabilities in fatigue crack propagation. The crack propagation acceleration right after the overload is not visible in the material response. Only the delay retardation and the gradual return to steady state rate behaviour is observed.

Using a trying and error procedure, constants of the modified Wheeler's model were identified for each specimen. Values are summarised in Table 3. The response of the model is superimposed to the experimental response, in Fig. 12. Good agreements between the experimental data and the modified Wheeler's model are observed. For

the metallic material of the Fão Bridge under consideration, the yield stress adopted was the monotonic yield stress of the material, σ_y = 220 MPa (from Jesus et al 2009).

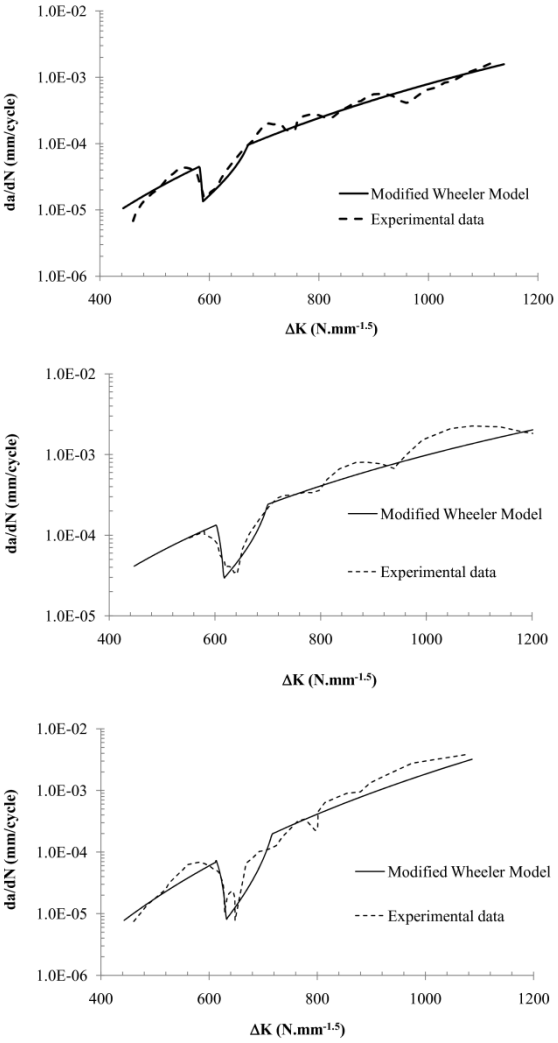

Fig. 12- Overload fatigue crack propagation data: experimental and numerical prediction.

Table 3 - Parameters of the modified Wheeler's model.

Spec.	n	α	q	ξ	C	m
CT1	0.6	0.2	1.0	0.17	1.02E-19	5.30
CT2	0.8	0.2	1.0	0.24	1.58E-15	3.94
CT3	1.2	0.2	1.0	0.28	1.37E-23	6.71

Note: da/dN in mm/cycle and ΔK in N.mm$^{-1.5}$

The analysis of the Table 3 allows some conclusions. The effective plastic zone size constant, α, is the same for the three specimens. This value falls within plane strain and plane stress proposed range. Since no acceleration immediately after the overload was observed the q value was assumed equal to unity for all cases. Parameters n and ξ almost doubled between the first and third specimen. The steady state fatigue crack propagation obtained for the three specimens is very distinct as can be observed by parameters C and m. These distinct stable state fatigue crack propagations make difficult any attempt to use all overload data together to derive the constants from the modified Wheeler model. Fig. 13 illustrates all experimental data plotted together. It is very clear a high scatter. This scatter is visible not only on the steady state fatigue crack growth but also on crack growth retardation rate levels.

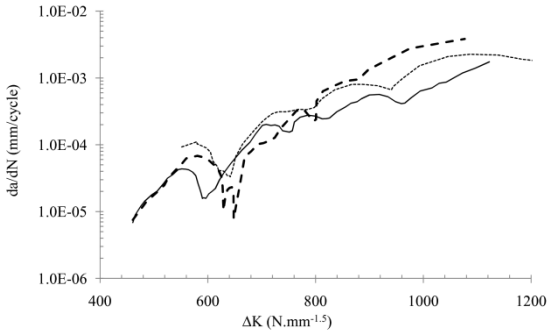

Fig. 13- Superposition of experimental crack growth rates.

5- CONCLUSIONS

Experimental fatigue crack growth data was derived for the puddle iron from the road Fão bridge under constant amplitude loading covering several stress R-Ratios. The Paris's equation was used to correlate the experimental data. Furthermore, the Walker's equation was used to improve the description of the stress R-ratio effects.

The constant amplitude fatigue crack growth rates of the material from the Fão bridge was compared with similar data of other bridge materials. Higher fatigue crack growth rates were observed for the material from this study.

The fatigue crack growth behaviour was also characterized for single overloads. A

crack growth retardation was verified right after the overload followed by gradual return to steady state. A modified version of the Wheeler model proposed by Yuen and Taheri was used to fit the experimental data. A good adjustment was verified for each individual test data. The same effective plastic zone size constant, α, was obtained for all specimens. For other constants, a range of variation was established.

The scatter is a markedly characteristic of the puddle iron investigated in this study, which is justified by the high level of heterogeneities. This characteristic difficult the assessment of the crack propagation behaviour under variable amplitude loading, since the effects of materials heterogeneities may mask the load sequential effects.

6- ACKNOWLEDGEMENTS

The authors acknowledge the Portuguese Science Foundation for the support through the research project PTDC/EME-PME/78833/2006.

7- REFERENCES

ASTM E647: ASTM STANDARD. 1999. Standard Test Method for Measurement of Fatigue Crack Growth Rates. American Society for Testing and Materials.

Correia, J.A.F.O., Jesus, A.M.P., Figueiredo, M.A.V., Ribeiro, A.S., Fernandes, A.A. 2008. Variability analysis of fatigue crack growth rates of materials from ancient Portuguese steel bridges, Proceedings of the Fourth International Conference on Bridge Maintenance, Safety and Management, Seoul, Korea, p. 1249-1301.

De Jesus, A.M.P., Silva, A.L., Silva, J.F., Maeiro, J.M., Silva, P.L.B.. 2009. Caracterização à fadiga do material da ponte metálica rodoviária de Fão, P.J.S. Cruz, T. Mendonça, L.C. Neves and L.O. Santos (eds), Proceedings of 1st Portuguese Conference on Safety and Rehabilitation of Bridges, Lisboa, Portugal, p. (III)175-182.

DiBattista, J.D., Adamson D.E.J., Kulak G.L. 1998. Evaluation of remaining fatigue life for riveted truss bridges, Canadian Journal of Civil Engineering, 25(4), p.678-691.

Geissler, K. 2002. Assessment of old steel bridges, Germany, Structural Engineering International, 12(4), p. 258-263.

Irwin, G.R. 1957. Analysis of Stresses and Strains Near the End of a Crack Tip Traversing a Plate, ASME Journal of Applied Mechanics, E24, p. 361–364.

Kim, S.-H., Lee, S.-W., Mha, H.-S. 2001. Fatigue reliability assessment of an existing steel railroad bridge, Engineering Structures, 23, p.1203-1211.

Kulak, G.L. 2000. Fatigue strength of riveted shear splices, Progress in Structural Engineering and Materials, 2(1), p. 110-119.

Miner, M. A. 1945. Cumulative Damage in Fatigue, ASME Journal of Applied Mechanics, 67, p. A159–A164.

Paasch, R.K., DePiero, A.H. 1999. Fatigue Crack Modeling in Bridge Deck Connection Details, Final Report SPR 380, Oregon Department of Transportation.

Paris, P.C., Erdogan, F. 1963. A critical analysis of crack propagation laws, Transactions of The ASME. Series E: Journal of Basic Engineering, 85, p. 528-534.

Walker, K. 1970. The Effect of Stress Ratio During Crack Propagation and fatigue for 2024-T3 and 7075-T6 Aluminum. Effects of Environment and Complex Load Histories on Fatigue Life, ASTM STP 462, American Society for Testing and Materials.

Wang, C.S., Chen, A.R., Chen, W.Z., Xu, Y. 2006. Application of probabilistic fracture mechanics in evaluation of existing riveted bridges, Bridge Structures, 2(4), p. 223-232.

Wang, X., Gao, Z., Zhao, T., Jiang, Y. 2009. An experimental study of the crack growth behaviour of 16MnR pressure vessel steel, Journal of Pressure Vessel Technology, 131, p. 021402-9.

Wheeler, O.E. 1972. Spectrum Loading and Crack Growth, ASME Journal of Basic Engineering, 94, p. 181–186.

Yuen, B.K.C., Taheri, F. 2006. Proposed modifications to the Wheeler retardation model for multiple overloading fatigue life prediction, International Journal of Fatigue, 8, p. 1803–1819.